06

Crystal structure, microstructure, piezoelectric and dielectric properties of high-temperature piezoceramics $Bi_{3-x}Nd_xTi_{1.5}W_{0.5}O_9$ ($x = 0$, 0.1, 0.2)

© S.V. Zubkov[1], I.A. Parinov[2], A.V. Nazarenko[2,3], Yu.A. Kuprina[1]

[1] Scientific Research Institute of Physics, Southern Federal University, Rostov-on-Don, Russia
[2] I.I. Vorovich Institute of Mathematics, Mechanics and Computer Science, Southern Federal University, Rostov-on-Don, Russia
[3] Southern Scientific Center, Russian Academy of Sciences, Rostov-on-Don, Russia

E-mail: svzubkov61@mail.ru

Received April 10, 2022
Revised April 10, 2022
Accepted April 11, 2022

A new series of perovskite-like oxides $Bi_{3-x}Nd_xTi_{1.5}W_{0.5}O_9$ ($x = 0$, 0.1, 0.2) has been synthesized by the method of high-temperature solid-state reaction. The X-ray diffraction study showed that the compounds are single-phase and have the structure of the family of Aurivillius phases with parameters close to the orthorhombic unit cell corresponding to the space group $A2_1am$. The relative permittivity $\varepsilon/\varepsilon_0$ and loss angle tangent $\mathrm{tg}\,\sigma$ are measured as functions of temperature at different frequencies. The piezoelectric modulus d_{33} was measured for the synthesized compounds. The microstructure of $Bi_{3-x}Nd_xTi_{1.5}W_{0.5}O_9$ ($x = 0$, 0.1, 0.2) was obtained. The study of the microstructure shows that the crystallites have a shape characteristic of Aurivillius phases.

Keywords: Aurivillius phases, $Bi_{2.8}Nd_{0.2}Ti_{1.5}W_{0.5}O_9$, activation energy E_a, Curie temperature T_C.

DOI: 10.21883/PSS.2022.10.54235.341

1. Introduction

In 1949 while studying the $Bi_2O_3-TiO_2$ system, V. Aurivillius established that the formation of $Bi_4Ti_3O_{12}$ oxide with a perovskite-type structure takes place in it [1]. Only ten years later, after the discovery by G.A. Smolensky, V.A. Isupov, and A.I. Agranovskaya of the ferroelectric properties of Bi_2PbNbO_9, a new stage in the study of compounds of this type (the family of Aurivillius phases) began [2]. Aurivillius phases form a large family of bismuth-containing perovskite-type layered compounds, whose chemical composition is described by the general formula $A_{m-1}Bi_2B_mO_{3m+3}$. The crystal structure of the Aurivillius phase family (APF) consists of alternating $[Bi_2O_2]^{2+}$ layers separated by m perovskite-like layers $[A_{m-1}B_mO_{3m+1}]^{2-}$, where A — ions with large radii have dodecahedral coordination, and positions B inside oxygen octahedra are occupied highly charged (3+ or more) cations with a small radius. The value m is determined by the number of perovskite layers $[A_{m-1}B_mO_{3m+1}]^{2-}$ located between the fluorite-like layers $[Bi_2O_2]^{2+}$, and can take an integer or half-integer values in the range from 1 to 6 (in Fig. 1 $m = 2, 3, 4$).

The layered ferroelectrics of the Aurivillius phase family are attracting much attention due to their high Curie temperature T_C [3–5]. The rapid development of piezoelectric devices for aerospace, aviation and nuclear power has increased the demand for piezoelectric materials capable of operating at elevated temperatures [6]. APF ferroelectrics also have excellent fatigue resistance and thermal stability properties [7]. However, the piezoelectric coefficient d_{33} of the APF is very low due to the high coercive field E_c and structural anisotropy [8]. Bismuth titanate-wolframate ($Bi_3Ti_{1.5}W_{0.5}O_9$, abbreviated as BTW) is one of the APF compounds with a high Curie temperature (760°C), but low piezoelectric coefficient (< 9 pC/N) [9]. Doping of APF compounds is a way to improve the piezoelectric properties of APF ceramics. The substitution of compound ions both in the A position and in the B position can significantly improve the properties of APF ceramics, including the piezoelectric properties. Substitution of an ion in the A position in APF compounds has a stronger effect on the piezoelectric properties than a substitution in the B position [10–12]. Previous studies have reported various impurities in the B position to improve the piezoelectric properties of Bi_3TiNbO_9 (BTN) ceramics. For example, substitution of W^{6+} ions with Ta^{5+} in the B position not only increases the piezoelectric activity ($d_{33} = 12.2$ pC/N), but also increases electrical resistivity [13,14]. In addition, the joint substitution of the Ti ion in the B position by Sc/Ta also increases the value of d_{33} from 6 to 12 pC/N [15]. However, only a few studies have reported the substitution of an ion at the A position in BTN-based ceramics to improve the piezoelectric properties [16–18]. In this work, we studied the effect of doping with Nd ions in the A position on the change in the piezoelectric properties of the $Bi_{3-x}Nd_xTi_{1.5}W_{0.5}O_9$ compound ($x = 0$, 0.1, 0.2). Bismuth titanate-wolframate $Bi_3Ti_{1.5}W_{0.5}O_9$ (BTW), was

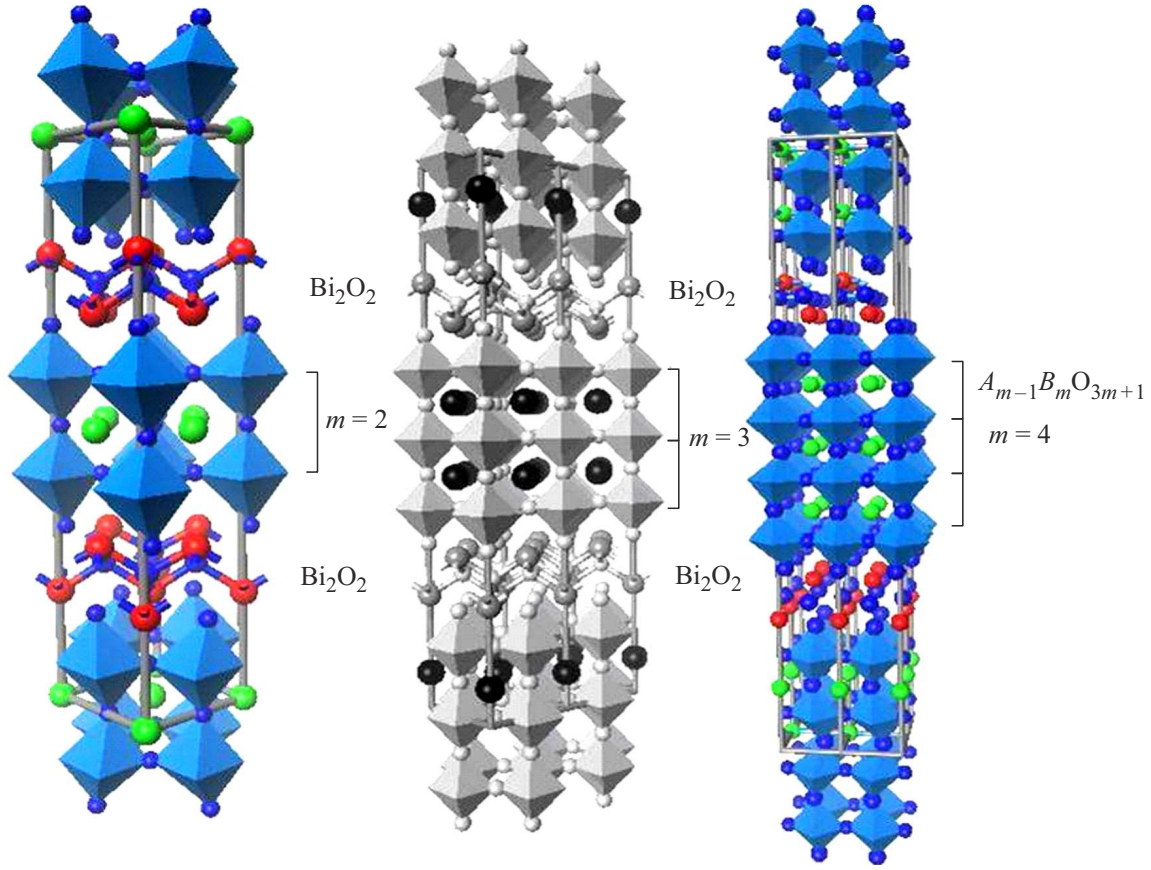

Figure 1. Aurivillius phase structure: *a*) $m = 2$, *b*) $m = 3$, *c*) $m = 4$.

first synthesized by Kikuchi in 1977 [19]. BTW refers to the APF with $m = 2$ and along with the high Curie temperature ($T_C = 760°C$) it also has a relatively large piezoelectric modulus ($d_{33} = 8$ pC/N). In the present work, bismuth ions in the *A* position were doped with neodymium ions. Early studies indicated that doping with a Nd ion at the *A* position of a rare earth element increases the piezoelectric activity of $Bi_4Ti_3O_{12}$ [20]. Ceramic $Bi_{3-x}Nd_xTi_{1.5}W_{0.5}O_9$ ($x = 0$, 0.1, 0.2) was synthesized by the solid-phase reaction. The crystal structure, microstructure, dielectric properties, piezoelectric properties, thermal stability and change in the porosity of ceramics have been studied.

2. Experiment

Polycrystalline samples with the structure of the Aurivillius phase (AP) $Bi_{3-x}Nd_xTi_{1.5}W_{0.5}O_9$ ($x = 0$, 0.1, 0.2) were synthesized by solid-state reaction of oxides Bi_2O_3, Nd_2O_3, TiO_2, WO_3. All original compounds were of analytic grade. After weighing in quantities corresponding to the stoichiometric composition and thorough grinding of the initial oxides with the addition of ethanol, the pressed samples were calcined at temperature of 770°C for 4 hours. The samples were annealed in a laboratory muffle furnace in air. The sample was then crushed, repeatedly fined and pressed into tablets of a diameter 10 mm and a thickness of 1.0−1.5 mm,followed by final synthesis at temperature of 1100°C (for 2 hours).

The X-ray pattern was recorded on a Rigaku Ultima IV diffractometer with an X-ray tube with a copper anode. The Cu $K_{\alpha1,\alpha2}$ radiation was separated from the total spectrum using a nickel filter. The X-ray pattern was measured in the range of angles 2θ from 10 to 60° with a scanning step of 0.02° and an exposure (intensity recording time) of 4 s per point. Analysis of the X-ray pattern profile, determining the position of the lines, their indexing (hkl), and refinement of the unit cell parameters were carried out using the PCW 2.4 program [21]. To measure the permittivity and electrical conductivity, electrodes were deposited on flat surfaces of APF samples in the form of disks 10 mm in diameter and about 1.5 mm thick, using Ag paste annealed at a temperature of 700°C (for 20 min). The temperature and frequency dependences of the dielectric characteristics were measured using an E7-20 immitance meter in the frequency range from 100 kHz to 1 MHz and in the temperature range from room temperature to 900°C. The sample was subjected to polarization in an oil bath at 145°C at a voltage of 35 kV/cm for 30 min. Photos of transverse chippings of $Bi_{3-x}Nd_xTi_{1.5}W_{0.5}O_9$ ($x = 0$, 0.1, 0.2) were obtained at the Collective Use Center of the SSC

Table 1. Lattice cell parameters a_0, b_0, c_0, V, as well as a_t — tetragonal period parameter, c' — height of the octahedron along the c axis, $\delta c'$ — deviation from the cubic shape, δb_0 — rhombic distortion, t — tolerance factor

Compound	a_0, Å	b_0, Å	c_0, Å	V, Å^3	c', Å	a_t, %	$\delta c'$, %	δb_0, %	t
$Bi_3Ti_{1.5}W_{0.5}O_9$	5.3861	5.3742	24.8572	719.51	3.7586	3.8043	−1.2	−0.2	0.9778
$Bi_{2.9}Nd_{0.1}Ti_{1.5}W_{0.5}O_9$	5.3902	5.3875	24.7116	717.6175	3.7067	3.81	−2.7	−0.05	0.9628
$Bi_{2.8}Nd_{0.2}Ti_{1.5}W_{0.5}O_9$	5.3935	5.3861	24.7668	719.4738	3.715	3.811	−2.51	−0.14	0.9616

RAS at KeyenceVK-9700 3D scanning laser microscope (wavelength 408 nm) (Japan). The photos were taken confocal in reflected light. The vertical scan step (Z axis) was 0.08 μm in „Real Peak Detection“ mode. The surface porosity of the transverse chipping was calculated as the ratio of the total area of pores visible in the image to the total surface area of the image.

3. Results and discussion

Powder X-ray diffraction patterns of all investigated $Bi_{3-x}Nd_xTi_{1.5}W_{0.5}O_9$ solid solutions ($x = 0$, 0.1, 0.2) correspond to single-phase APFs with $m = 2$ and do not contain additional reflections. These compounds are isostructural to the known perovskite-like APF oxide $Bi_3Ti_{1.5}W_{0.5}O_9$. It was found that all synthesized APs crystallize in an orthorhombic system with unit cell space group $A2_1am$ (№ 36 in PCW 2.4). X-ray patterns of all compounds correspond to APF with $m = 2$. Figure 2 shows the experimental powder X-ray diffraction patterns of the compounds under study.

The lattice cell parameters (lattice constants a_0, b_0, c_0 and volume V) were determined from X-ray diffraction data; they are listed in Table 1. Table 1 also shows the parameters of orthorhombic and tetragonal deformations: average tetragonal period $a_t = (a_0 + b_0)/(2\sqrt{2})$, tolerance factor t, average thickness of a single perovskite-like layer $c' = 3c/(8 + 6m)$, cell deviation from the cubic shape (that is, elongation or contraction) $\delta c' = (c' - a_t)/a_t$, orthorhombic deformation $\delta b_0 = (b_0 - a_0)/a_0$ [22,23].

The obtained unit cell parameters of the studied APF samples $Bi_{3-x}Nd_xTi_{1.5}W_{0.5}O_9$ ($x = 0$, 0.1, 0.2) are close to those previously determined for $Bi_3Ti_{1.5}W_{0.5}O_9$: $a = 5.4018(2)$ Å, $b = 5.3727(4)$ Å, $c = 24.9388(1)$ Å [24].

To estimate the degree of distortion of the ideal perovskite structure, we determined the tolerance factor t. The tolerance factor was introduced by Goldschmidt [25] as a geometric criterion that determines the degree of stability and distortion of the crystal structure:

$$t = (R_A + R_O)/\left[\sqrt{2}(R_B + R_O)\right], \qquad (1)$$

where R_A and R_B are the radii of the cations in positions A and B, respectively; R_O is ionic radius of oxygen. In this work, the tolerance factor was calculated taking into account the Shannon ionic radii [26] for the corresponding coordination numbers (CN): for

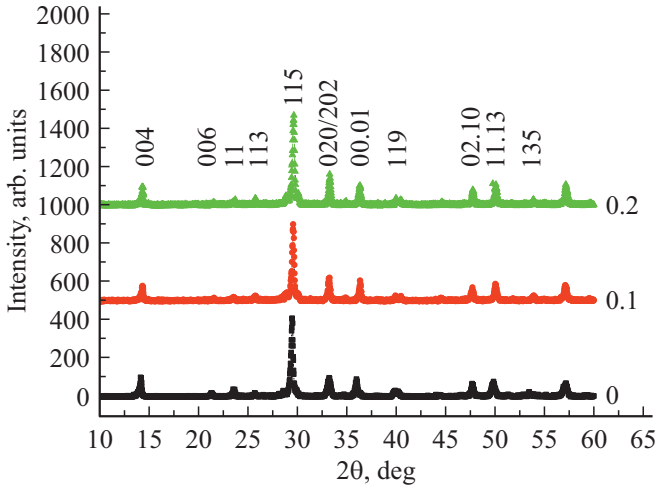

Figure 2. Experimental X-ray diffraction patterns of ceramics $Bi_{3-x}Nd_xTi_{1.5}W_{0.5}O_9$ ($x = 0$, 0.1, 0.2).

O^{2-} with CN equal to six, $R_O = 1.40$ Å; for Nd^{3+} with CN equal to twelve, $R_{Nd3+} = 1.27$ Å; for W^{6+} with CN equal to six, $RF_{W6+} = 0.6$ Å; for Ti^{4+} with CN equal to six, $R_{Ti4+} = 0.605$ Å. Shannon did not provide an ionic radius Bi^{3+} for coordination with the CN equal to twelve. Therefore, its value was determined from the ionic radius for CN equal to eight ($R_{Bi3+} = 1.17$ Å) multiplied by the approximation factor 1.179, then for Bi^{3+} with CN equal to twelve, we obtained $R_{Bi3+} = 1.38$ Å.

Figure 3, *a*, *b*, c shows images of $Bi_{3-x}Nd_xTi_{1.5}W_{0.5}O_9$ ceramics ($x = 0$, 0.1, 0.2) obtained with laser microscope. In contrast to the concentration $x = 0.2$ for compositions with $x = 0$ and $x = 0.1$, the grain morphology could be fixed only in large-sized technological pores.

In all cases, it can be seen that the grains have a lamellar shape, which is a typical characteristic of APF polycrystalline ceramics. That anisotropic character is explained by the fact that, due to the existence of rigid layers $(Bi_2O_2)^{2+}$, the grain growth rate in the $a - b$ plane is much higher than in the direction of the crystallographic axis c. Plane $a - b$ is parallel to the plane of lamellar grains, and the axis c is parallel to the direction of the axis of lamellar grains. On the obtained images of ceramics $Bi_{3-x}Nd_xTi_{1.5}W_{0.5}O_9$ at $x = 0$ (*a*), 0.1 (*b*), 0.2 (*c*) mixed lamellar grains of different orientations are added together.

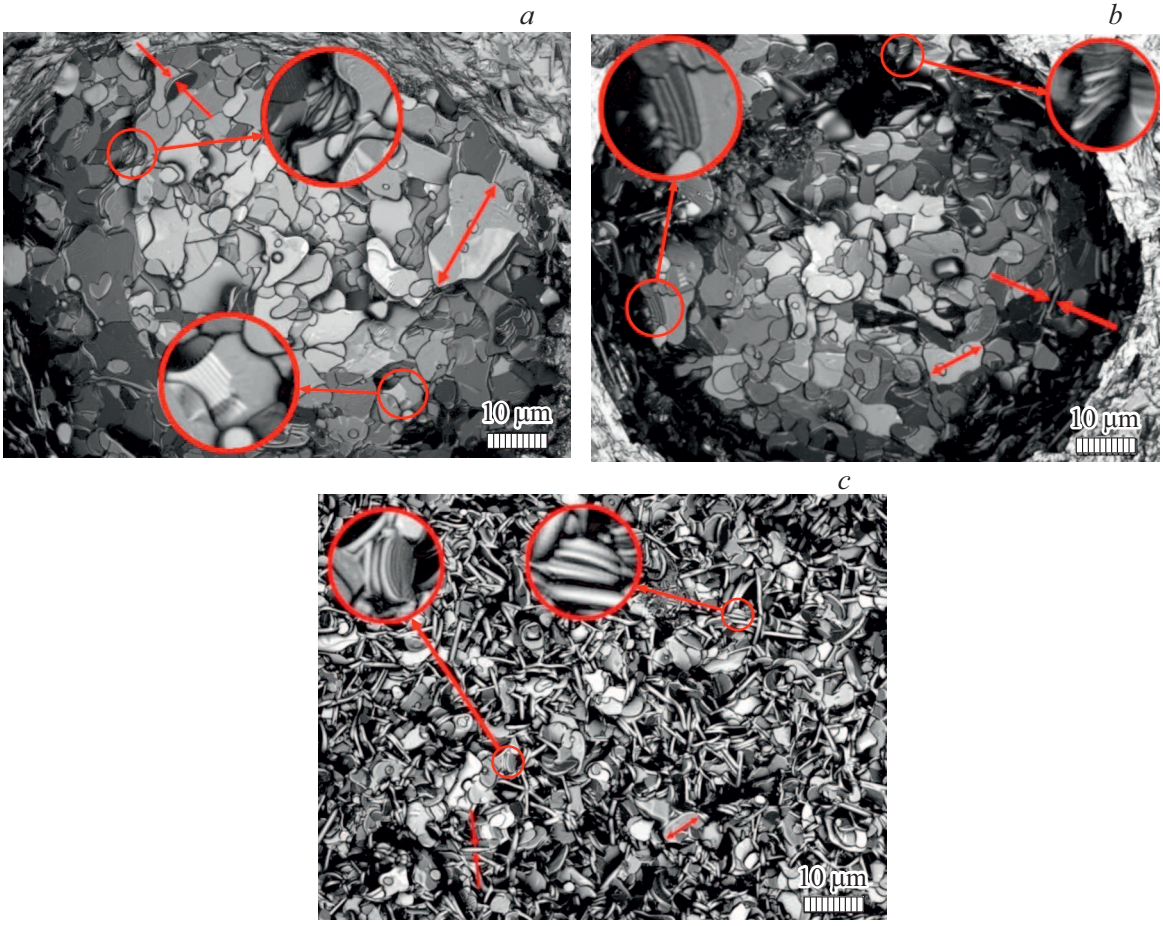

Figure 3. Images of the surface of transverse chippings of $Bi_{3-x}Nd_xTi_{1.5}W_{0.5}O_9$ ceramics at $x = 0$ (a), 0.1 (b), 0.2 (c).

In the nature of the arrangement of crystallites, stacks of thin ($\sim 0.5\,\mu$m) lamellar grains are observed (Fig. 3, highlighted areas), which is also characteristic of ceramics of the AP family. It can be seen that the grain boundaries are clear, and there are no inclusions in the interlayers between them. Apparently, this means that ceramics were sintered predominantly without vitreous phases of eutectic origin.

The size estimation was carried out taking into account all visible grains, regardless of their relative position. In this case, the line of the greatest length was chosen (Fig. 2, arrows). Figure 4 shows a histogram of grain size distribution as a percentage of their total number on the visible surface.

It can be noted that the bulk of the grains (about 70%) for all concentrations under consideration is in the range of $2-6\,\mu$m. However, if for $x = 0$ in a given „corridor“ the distribution is more or less uniform, then for compositions with $x = 0.1$, 0.2 it narrows to $2-4.5\,\mu$m, which says about a decrease in the average size of the plates with an increase in the concentration of Nd. It can be assumed that the grain growth rate of ceramics $Bi_{3-x}Nd_xTi_{1.5}W_{0.5}O_9$ ($x = 0.1$, 0.2) can be partially suppressed by the corresponding amount of Nd ion. This change can be explained by a decrease in the concentration of oxygen vacancies after appropriate doping with neodymium, which reduces the diffusion coefficient in the lattice and, accordingly, limits the mass transfer process.

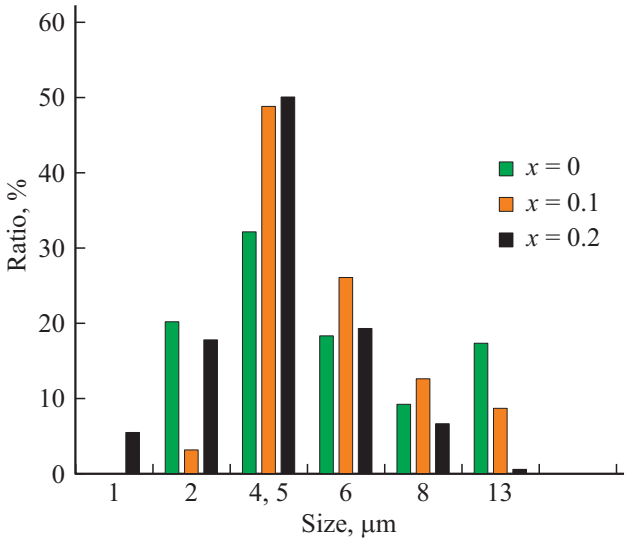

Figure 4. Grain size distribution in $Bi_{3-x}Nd_xTi_{1.5}W_{0.5}O_9$ ceramics ($x = 0$, 0.1, 0.2).

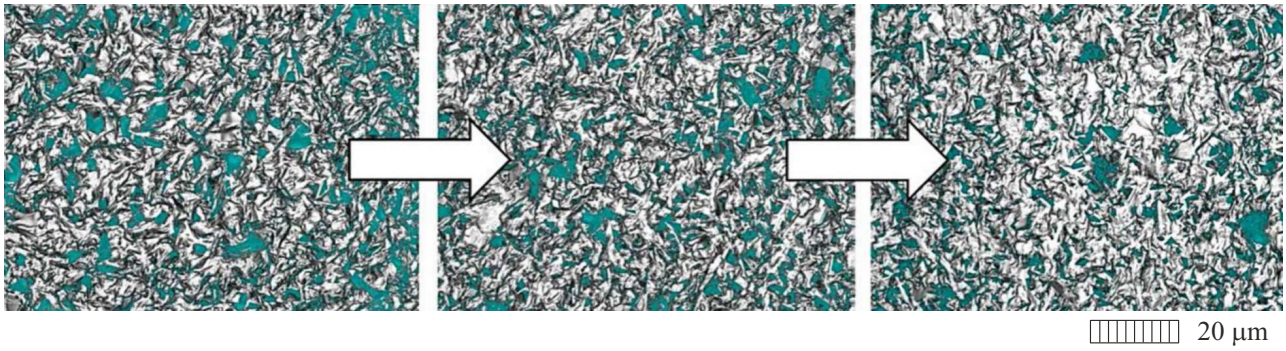

Figure 5. Estimation of porosity in $Bi_{3-x}Nd_xTi_{1.5}W_{0.5}O_9$ ceramics (from right to left $x = 0$, 0.1, 0.2).

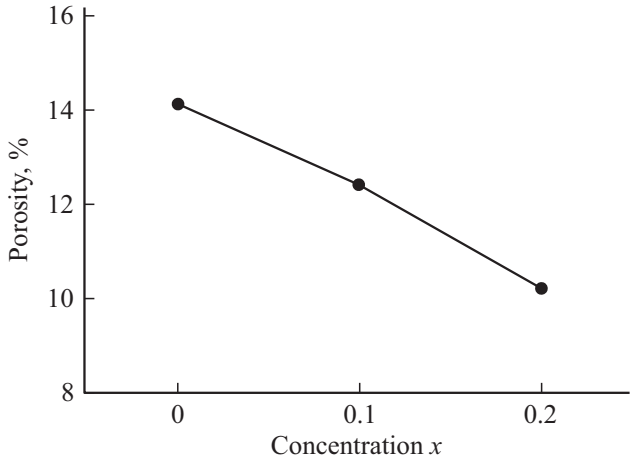

Figure 6. Dependence of surface porosity of chippings of ceramics $Bi_{3-x}Nd_xTi_{1.5}W_{0.5}O_9$ ($x = 0$, 0.1, 0.2) on the concentration Nd.

The general decrease in the size of crystallites contributes to their denser arrangement in ceramics. To estimate the porosity, images of sections of transverse chippings of the same size, on which only pores of a diffusion nature are present, were obtained separately. Since the microscope forms a confocal image and, according to the intensity of the received signal, can form a surface relief, further analysis of the existing pores was carried out under the same conditions by extraction the weakest reflections. Figure 5 shows the results of the analysis for evolution of grain packing density in ceramics $Bi_{3-x}Nd_xTi_{1.5}W_{0.5}O_9$ ($x = 0$, 0.1, 0.2) with increasing Nd concentration.

The calculation of the ratio of the area occupied by pores to the total area of the image showed that the surface porosity decreases with increasing Nd concentration from 14.1% to 10.2% (Fig. 6).

This, together with the high density and low porosity of ceramics, as well as the fact of absence of a glassy phase allows us to conclude that the chosen temperature conditions for sintering (1100°C) are optimal.

Figure 7 shows the temperature dependences of the relative permittivity $\varepsilon(T)$ and the dielectric loss tangent for $Bi_{3-x}Nd_xTi_{1.5}W_{0.5}O_9$ ($x = 0$, 0.1, 0.2) at frequency from 100 kHz to 1 MHz.

The maximum permittivity corresponding to the phase transition of a ferroelectric to a paraelectric (at T_C) is clearly observed for all compounds of the synthesized AP series $Bi_{3-x}Nd_xTi_{1.5}W_{0.5}O_9$ ($x = 0$, 0.1, 0.2) at frequencies from 100 kHz to 1 MHz. The intensity of the peak value of the relative permittivity slightly decreases with increasing neodymium concentration. The values of the dielectric loss tangent for $Bi_{3-x}Nd_xTi_{1.5}W_{0.5}O_9$ ($x = 0$, 0.1) are approximately the same, while for $Bi_{3-x}Nd_xTi_{1.5}W_{0.5}O_9$ ($x = 0.2$) are halved. The dielectric losses are very small in the temperature range from 300°C for $Bi_3Ti_{1.5}W_{0.5}O_9$ and up to 400°C for $Bi_{2.8}Nd_{0.2}Ti_{1.5}W_{0.5}O_9$. With increase in temperature, dielectric losses increase, have a clearly defined maximum at all measured frequencies, and then sharply decrease. The dielectric loss minimum usually precedes the dielectric peak by 5°C, although this is not always the case. With further increase in temperature, the dielectric losses sharply increase.

Figure 8 shows the dependence of the piezoelectric constant d_{33} $Bi_2.8Nd0.2Ti_{1.5}W_{0.5}O_9$ on temperature. The $Bi_2.8Nd0.2Ti_{1.5}W_{0.5}O_9$ ceramic exhibits good stability after heating to 630°C. Table 2 shows the piezoelectric modulus d_{33} for $Bi_{3-x}Nd_xTi_{1.5}W_{0.5}O_9$ ($x = 0$, 0.1, 0.2).

The activation energy E_a is determined from the Arrhenius equation:

$$\sigma = (A/T)\exp[-E_a/(kT)], \qquad (2)$$

where σ is electrical conductivity, k is Boltzmann constant, A is constant. Typical dependence of $\ln\sigma$ on $1/T$ at a frequency of 100 kHz, which was used to determine the activation energy Ea, is shown in Fig. 9 for AP $Bi_{3-x}Nd_xTi_{1.5}W_{0.5}O_9$ ($x = 0$, 0.1, 0.2). Compounds $Bi_{3-x}Nd_xTi_{1.5}W_{0.5}O_9$ ($x = 0$, 0.1, 0.2) have two temperature ranges in which the activation energy E_a differs significantly in value. At low temperatures, electrical conductivity is determined mainly by impurity defects with very low activation energies on the order of several hundredths of eV. For compounds $Bi_{3-x}Nd_xTi_{1.5}W_{0.5}O_9$ ($x = 0$, 0.1, 0.2), we

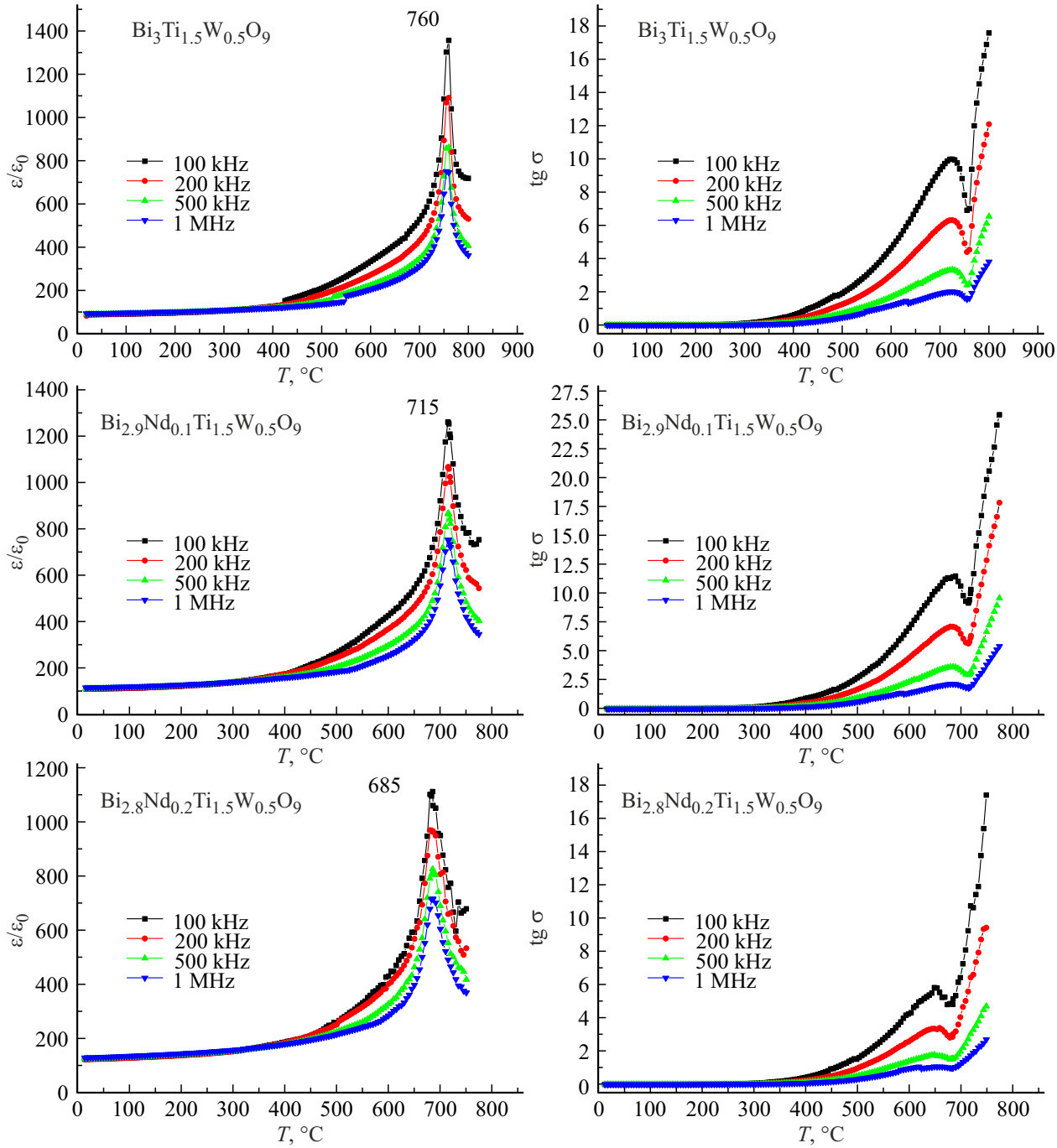

Figure 7. Temperature dependences of relative permittivity $\varepsilon/\varepsilon_0$ and loss tangent $\mathrm{tg}\,\delta$ for AP $Bi_{3-x}Nd_xTi_{1.5}W_{0.5}O_9$ ($x = 0$, 0.1, 0.2) at frequency from 100 kHz to 1 MHz.

Table 2. Dielectric characteristics of $Bi_3Ti_{1.5}W_{0.5}O_9$: Curie temperature T_C, piezoelectric modulus d_{33}, relative permittivity $\varepsilon/\varepsilon_0$, activation energies E_a at high and low temperatures (separated by commas)

Compound	T_C, °C	d_{33}, pC/N	$\varepsilon/\varepsilon_0$	E_a, eV
$Bi_3Ti_{1.5}W_{0.5}O_9$	760	8	1000	0.67, 0.06
$Bi_{2.9}Nd_{0.1}Ti_{1.5}W_{0.5}O_9$	715	10	1284	0.7, 0.09
$Bi_{2.8}Nd_{0.2}Ti_{1.5}W_{0.5}O_9$	685	15	1120	0.73, 0.07

observe a region with pronounced impurity conductivity in the temperature range from 20°C to 400°C.

Figure 9 shows the dependence of the logarithm of conductivity on temperature. When doping $Bi_{3-x}Nd_xTi_{1.5}W_{0.5}O_9$ ($x = 0.0$, 0.1, 0.2) with neodymium, the activation energy E_a in the low-temperature and high-temperature regions, as follows from Table 2, practically does not change. The invariance of the activation energy indicates the constancy of the na-

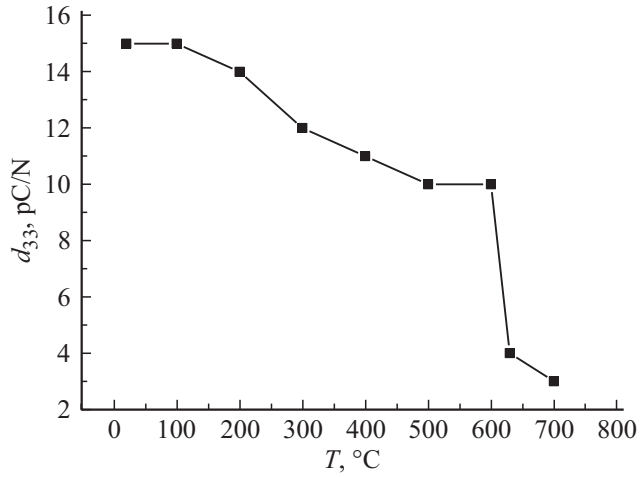

Figure 8. Temperature dependence of the piezoelectric constant d_{33} $Bi_{2.8}Nd_{0.2}Ti_{1.5}W_{0.5}O_9$.

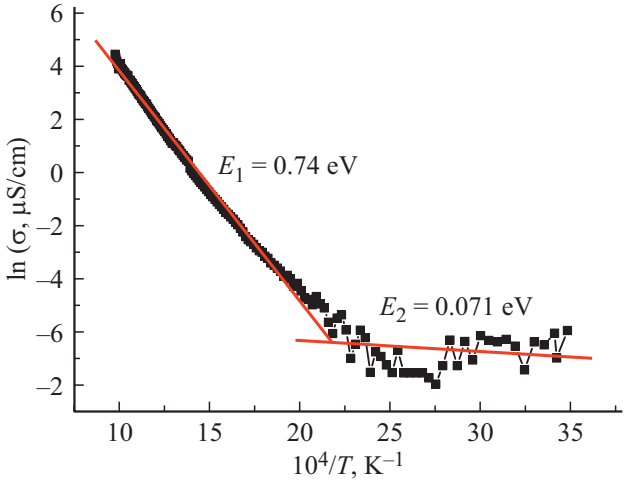

Figure 9. Dependence of $\ln\sigma$ on 10000/T for the $Bi_{2.8}Nd_{0.2}Ti_{1.5}W_{0.5}O_9$ sample at a frequency of 100 kHz.

ture of conductivity in the synthesized series of compounds.

4. Conclusion

Lamellar bismuth ceramic $Bi_{3-x}Nd_xTi_{1.5}W_{0.5}O_9$ ($x = 0$, 0.1, 0.2) was synthesized using a conventional solid phase reaction process. X-ray patterns show that all samples have a single lamellar bismuth structure. The temperature of the paraelectric-ferroelectric phase transition TS for $Bi_{3-x}Nd_xTi_{1.5}W_{0.5}O_9$ ($x = 0.1$, 0.2). was determined. For $Bi_{2.9}Nd_{0.1}Ti_{1.5}W_{0.5}O_9$ the Curie temperature is $T_C = 715°C$, for $Bi_{2.8}Nd_{0.2}Ti_{1.5}W_{0.5}O_9$ the Curie temperature is $T_C = 685°C$. The optimal sintering temperature $T = 1100°C$ was determined. It can be seen from the SEM that with an increase in the Nd content, the grain growth decreases. The decrease in grain growth is associated with decrease in oxygen vacancies. Decrease in grain oxygen vacancies leads to decrease in conductivity and, as a consequence, to decrease in tanσ losses and an increase in d_{33}. Ceramic composition $Bi_{2.8}Nd_{0.2}Ti_{1.5}W_{0.5}O_9$ exhibits optimized electrical performance with high d_{33} equal to 15 pC/N, high T_C equal to 685°C, and low tanσ. Moreover, d_{33} of ceramics $Bi_{2.8}Nd_{0.2}Ti_{1.5}W_{0.5}O_9$ remains at a level of 66% of the initial value at an annealing temperature above 600°C. In the sample doped with Nd, the concentration of oxygen vacancies decreases, and the electrical characteristics also improve. All these results indicate that the $Bi_{2.8}Nd_{0.2}Ti_{1.5}W_{0.5}O_9$ is new lead-free piezo material with high Curie temperature.

Acknowledgments

The equipment of the SFedU was used. The authors are grateful for the support of the Southern Federal University, grant No. 21-19-00423 of the Russian Science Foundation.

Conflict of interest

The authors declare that they have no conflict of interest.

References

[1] B. Aurivillius. Ark. Kemi **54**, 463 (1949).
[2] G.A. Smolensky, V.A. Isupov, A.I. Agranovskaya. FTT **1**, 169 (1959) (in Russian).
[3] E.C. Subbarao. J. Am. Ceram. Soc. **45**, 166 (1962).
[4] E.C. Subbarao. Chem. Phys. **34**, 695 (1961).
[5] S.V. Zubkov, V.G. Vlasenko. FTT **59**, 2303 (2017) (in Russian).
[6] S.J. Zhang, F.P. Yu. J. Am. Ceram. Soc. **94**, 3153 (2011).
[7] B.H. Park, B.S. Kang, S.D. Bu, T.W. Noh, J. Lee, W. Jo. Nature **401**, 682 (1999).
[8] R.E. Newnham, R.W. Wolfe, J.F. Dorrian. Mater. Res. Bull. **6**, 1029 (1971).
[9] . S.V. Zubkov, I.A. Parinov, Yu.A. Kuprina, A.V. Nazarenko. FTT **64**, *6*, 652 (2022) (in Russian).
[10] X. Zhang, H. Yan, M.J. Reece. J. Am. Ceram. Soc. **91**, 2928 (2010).
[11] H. Yan, C. Li, J. Zhou, W. Zhu, L. He, Y. Song, Y. Yu. Jpn. J. Appl. Phys. **40**, 6501 (2014).
[12] Yu.E. Kitaev, M.I. Aroyo, J.M. Perez-Mato. Phys. Rev. B **75**, 064110 (2007).
[13] Z. Peng, D. Yan, Q. Chen, D. Xin, D. Liu, D. Xiao, J. Zhu. Appl. Phys. **14**, 1861 (2014).
[14] Z. Zhou, X. Dong, H. Chen. J. Am. Ceram. Soc. **89**, 1756 (2006).
[15] Z.G. Gai, M.L. Zhao, W.B. Su, C.L. Wang, J. Liu, J.L. Zhang. J. Electroceramics **31**, 143 (2013).
[16] H. Zhang, H. Yan, M.J. Reece. J. Appl. Phys. **106**, 044106 (2009).
[17] S.V. Zubkov, V.G. Vlasenko. FTT **59**, *12*, 2303 (2017) (in Russian).
[18] J. Yuan, R. Nie, Q. Chen, D. Xiao, J. Zhu. Mater. Res. Bull. **115**, 70 (2019).
[19] T. Kikuchi. J. Alloys Compd. **48**, 319 (1976).

[20] S. Kim, J.S. Lee, H.J. Lee, C.W. Ahn, I.W. Kim, M.S. Jang. J. Electroceramics **21**, 633 (2008).
[21] W.Kraus, G.Nolze. PowderCell for Windows 2.39. Federal Institute for Materials Research and Testing, Berlin (1999).
[22] V.A. Isupov. Ferroelectrics **189**, 211 (1996).
[23] V.A. Isupov. Neorgan. materialy **421**, 353 (2006) (in Russian).
[24] N.C. Hyatt, I.M. Reaney, S.K. Knight. Phys. Rev. B **71**, 024119 (2005).
[25] V.M. Goldschmidt. Geochemische Verteilungsgesetze der Elemente. J. Dybwad, Oslo (1927).
[26] R.D. Shannon. Acta Crystallogr. A **32**, 75 (1976).